Article

Cell Reports

Predicting Drug Response in Human Prostate Cancer from Preclinical Analysis of In Vivo Mouse Models

Graphical Abstract

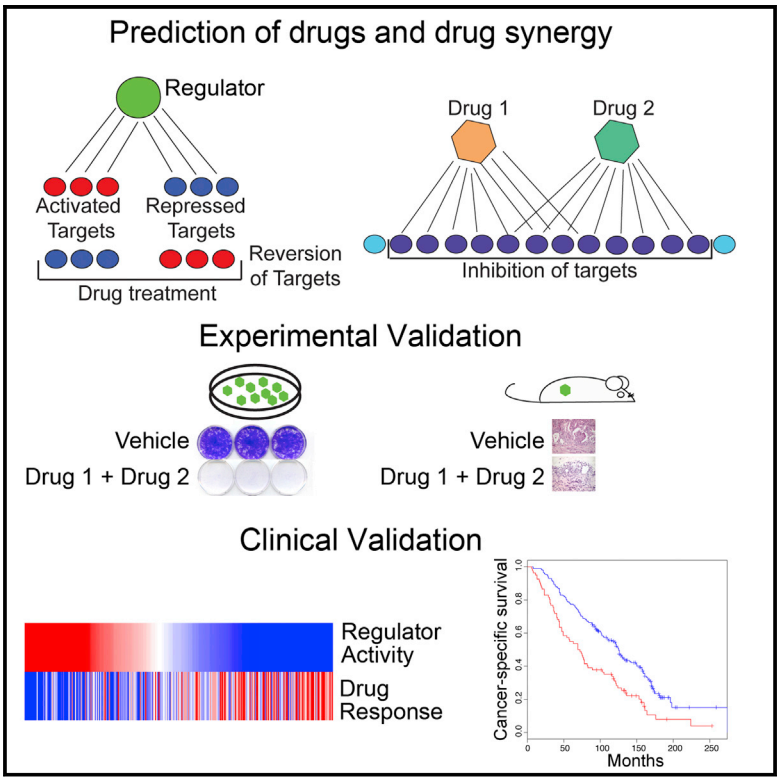

Authors

Antonina Mitrofanova, Alvaro Aytes, Min Zou, Michael M. Shen, Cory Abate-Shen, Andrea Califano

Correspondence

cabateshen@columbia.edu (C.A.-S.), califano@c2b2.columbia.edu (A.C.)

In Brief

Mitrofanova et al. describe a computational method using in vivo data from mouse models to identify drug combinations for human cancer treatment. They identify a drug combination that inhibits a key cancer dependency and show that genes responsive to treatment in mice identify human patients likely to benefit from treatment.

Highlights

- Computational method uses in vivo data from mice to predict drugs for human cancer
- Method predicts optimal drug combinations using data from single agents
- Demonstrates efficacy of co-targeting PI3 and MAP kinases for prostate cancer
- Generalizable method to use mouse preclinical data to inform human cancer treatment

Accession Numbers

GSE69211
GSE69213

Mitrofanova et al., 2015, Cell Reports *12*, 2060–2071
September 29, 2015
http://dx.doi.org/10.1016/j.celrep.2015.08.051

OPEN ACCESS
CellPress

Cell Reports
Article

Predicting Drug Response in Human Prostate Cancer from Preclinical Analysis of In Vivo Mouse Models

Antonina Mitrofanova,[1,8] Alvaro Aytes,[2,8] Min Zou,[2] Michael M. Shen,[1,2,3,4,7] Cory Abate-Shen,[1,2,5,7,*] and Andrea Califano[1,6,7,*]

[1]Department of Systems Biology
[2]Department of Urology
[3]Department of Medicine
[4]Department of Genetics and Development
[5]Department of Pathology and Cell Biology
[6]Department of Biochemistry and Molecular Biophysics
[7]Institute of Cancer Genetics
Herbert Irving Comprehensive Cancer Center, Columbia University Medical Center, New York, NY 10032, USA
[8]Co-first author
*Correspondence: cabateshen@columbia.edu (C.A.-S.), califano@c2b2.columbia.edu (A.C.)
http://dx.doi.org/10.1016/j.celrep.2015.08.051

SUMMARY

Although genetically engineered mouse (GEM) models are often used to evaluate cancer therapies, extrapolation of such preclinical data to human cancer can be challenging. Here, we introduce an approach that uses drug perturbation data from GEM models to predict drug efficacy in human cancer. Network-based analysis of expression profiles from in vivo treatment of GEM models identified drugs and drug combinations that inhibit the activity of FOXM1 and CENPF, which are master regulators of prostate cancer malignancy. Validation of mouse and human prostate cancer models confirmed the specificity and synergy of a predicted drug combination to abrogate FOXM1/CENPF activity and inhibit tumorigenicity. Network-based analysis of treatment signatures from GEM models identified treatment-responsive genes in human prostate cancer that are potential biomarkers of patient response. More generally, this approach allows systematic identification of drugs that inhibit tumor dependencies, thereby improving the utility of GEM models for prioritizing drugs for clinical evaluation.

INTRODUCTION

Recent large-scale genomic analyses have led to the identification of "actionable" driver genes of specific cancers that are therapeutically accessible, including oncogene and non-oncogene dependencies (Al-Lazikani et al., 2012; Garraway and Lander, 2013; Luo et al., 2009; Rubio-Perez et al., 2015). However, the accurate and efficient identification of drugs and drug combinations that inhibit such drivers within specific tumor contexts represents a major challenge, particularly for transcriptional regulators that, in general, are pharmacologically inaccessible. Genetically engineered mouse (GEM) models are well suited to empower investigations of targeted inhibitors in the context of the native tumor microenvironment in vivo (Abate-Shen and Pandolfi, 2013; Politi and Pao, 2011; Sharpless and Depinho, 2006). However, species differences with respect to tumor histology, physiology, pharmacology, and metabolism often preclude direct extrapolation of preclinical findings from mouse models to human cancer.

In the current study, we introduce an innovative regulatory-network-based method that uses expression profiles from drug-treated GEM models to predict drugs and drug combinations that specifically inhibit the activity of established human cancer dependencies. We focus this proof-of-concept study on prostate cancer, a disease characterized by heterogeneity of its causal mechanisms and range of disease outcomes (Chang et al., 2014; Cooperberg et al., 2005; Roychowdhury and Chinnaiyan, 2013; Shen and Abate-Shen, 2010). In particular, while most locally invasive prostate tumors are curable, recurrent or aggressive tumors initially respond to androgen deprivation therapy but ultimately relapse to castration-resistant metastatic disease, which is nearly always fatal (Ryan and Tindall, 2011; Scher and Sawyers, 2005). While treatment options for castration-resistant metastatic prostate cancer have significantly improved in recent years (Mukherji et al., 2014; Rathkopf and Scher, 2013; Wong et al., 2014), none of the available treatments are as yet curative.

We have recently generated genome-wide reverse-engineered regulatory networks (henceforth "interactomes") for both mouse and human prostate cancer (Aytes et al., 2014). Interrogation of these interactomes identified FOXM1 and CENPF as master regulators (i.e., key driver genes), which function synergistically to elicit synthetic lethality and are robust predictors of poor patient outcome (Aytes et al., 2014). Here, we show that interrogation of in vivo drug perturbation signatures from GEM models represents an effective strategy for systematic identification of specific drugs and drug combinations that

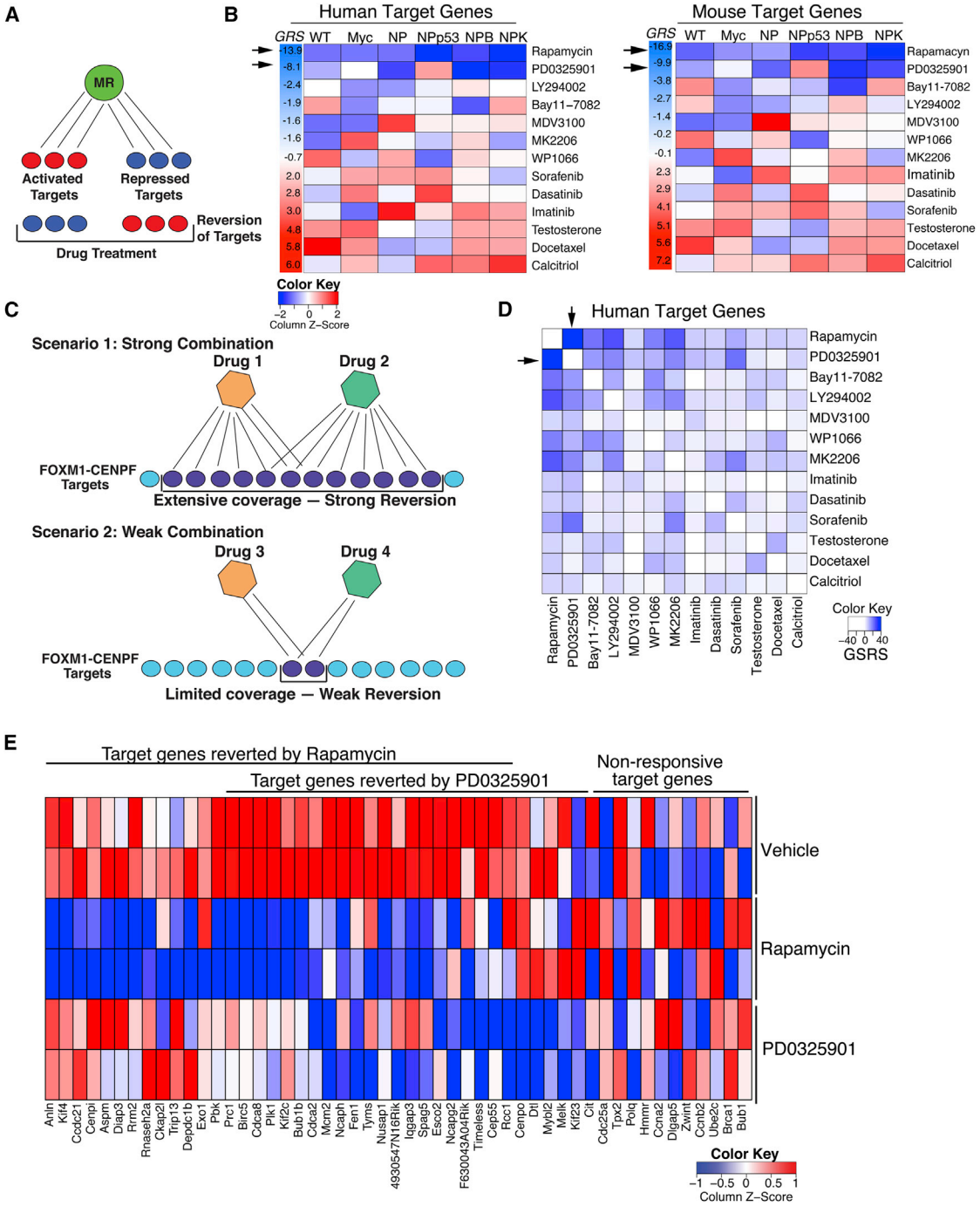

Figure 1. Computational Prediction of Drugs that Inhibit FOXM1/CENPF Activity In Vivo

(A) Shown is the strategy for prediction of single drugs. Drug reversion scores were calculated based on the degree to which target genes that are activated (red) by a master regulator (MR) are inhibited (blue) following drug treatment, and conversely, the degree to which target genes that are repressed (blue) by the MR are activated (red) following drug treatment (see Supplemental Experimental Procedures).

(B) Heatmap representations of GSEA used to calculate drug reversion scores across a series of GEM models with a series of drugs, as indicated (see Supplemental Experimental Procedures). GSEA were done using the mouse in vivo drug perturbation signatures as the reference and human or mouse FOXM1/CENPF target genes inferred from their respective prostate cancer interactomes, as indicated, as the query gene set. Global reversion scores (GRSs) were calculated for each drug by combining the individual NES for each GEM model using a metric based on the Stouffer integration formulation (see Supplemental Experimental Procedures). Arrows point to the two drugs with the highest GRSs.

(C) Shown is the strategy for prediction of drug synergy. Pairwise combinations of data from individual drug treatments (as in A) were assessed to predict drugs that effectively revert FOXM1/CENPF target genes when used in combination. Scenario 1 illustrates two drugs that inhibit (i.e., revert) many target

(legend continued on next page)

inhibit the transcriptional activity of FOXM1/CENPF. Strikingly, drug combinations that revert transcriptional activity of these proteins are highly effective in abrogating tumorigenesis in vivo and well correlated with patient outcome. We propose that this computational method can be generalized for more effective utilization of preclinical data from GEM models to predict optimal drugs and drug combinations and thereby dramatically improve the utilization of GEM models to prioritize compounds for clinical investigation.

RESULTS

Systematic Inference of FOXM1/CENPF Inhibitors In Vivo

The current methodology is predicated on our previous analyses showing that expression of the target genes of a given master regulator (MR) (its regulon) represents an effective reporter to predict the activity of the MR for a given cancer phenotype (Aytes et al., 2014; Carro et al., 2010; Chen et al., 2014). Here, we have extended this concept to evaluate whether such regulon can be used as a reporter to quantitatively measure the ability of a drug or drug combination to inhibit the activity of the corresponding MR. In general, reversion of MR activity would correspond to the ability of a given drug to *downregulate* its *activated* target genes and *upregulate* its *repressed* targets (Figure 1A). As a proof of concept for this approach, we evaluated drugs for their ability to inhibit the master regulator pair, FOXM1/CENPF, which we have previously established to be a key synthetic lethal dependency of prostate tumor malignancy (Aytes et al., 2014). In particular, we tested whether candidate therapeutic agents could be prioritized based on in vivo perturbation by assessing their ability to "reverse" the FOXM1/CENPF regulon. We focused on the activated shared targets of FOXM1/CENPF, since the number of repressed targets is too few for analysis. However, both activated and repressed targets may be used in general.

To assess this strategy, we used a drug perturbation dataset that includes drugs with known prostate cancer relevance, such as those that inhibit the androgen receptor, or key signaling pathways such as phosphatidylinositol 3-kinase (PI3K)/mTOR or MAP kinase or standard chemotherapy (Aytes et al., 2014; see Supplemental Experimental Procedures). In vivo drug perturbation studies were performed using multiple GEM models representative of advanced prostate cancer (Aytes et al., 2014; see Supplemental Experimental Procedures) to avoid potential bias introduced by any individual model. The in vivo drug perturbation data were analyzed by gene set enrichment analysis (GSEA) (Subramanian et al., 2005) to assess the inhibition (i.e., reversion) of FOXM1/CENPF shared target genes; analyses were performed separately for the mouse and human targets (Figure 1B). Using GSEA, we obtained a normalized enrichment score (NES) for each drug signature and each GEM model, which we define as the reversion score ($RS_{FOXM1/CENPF}$), to assess the compound's ability to inhibit FOXM1/CENPF activity in a specific GEM model (Table S1). From these analyses, a global reversion score ($GRS_{FOXM1/CENPF}$) was assigned for each drug by integrating each of the GEM-specific $RS_{FOXM1/CENPF}$ scores, using a metric based on Stouffer's integration formulation (Whitlock, 2005) (Figure 1B; Figure S1; Supplemental Experimental Procedures). Thus, drugs that most effectively inhibit FOXM1/CENPF activity are those having the most negative $GRS_{FOXM1/CENPF}$. Notably, FOXM1/CENPF target genes from either mouse or human yielded equivalent $GRS_{FOXM1/CENPF}$ (Figure 1B; Table S1), indicating conservation of the predicted drug response between mouse and human prostate cancer.

Among the individual drugs tested in the GEM models, the two with the most significant negative $GRS_{FOXM1/CENPF}$ were rapamycin and PD0325901. These drugs inhibit the PI3K/mTOR and MAP kinase signaling pathways, respectively, which are frequently dysregulated in advanced prostate cancer (Aytes et al., 2013; Kinkade et al., 2008; Taylor et al., 2010). Specifically, the GRSs for rapamycin were $GRS_H = -13.9$ (human targets) and $GRS_M = -16.9$ (mouse targets) and for PD0325901 were $GRS_H = -8.1$ and $GRS_M = -9.9$ (Figure 1B; Table S1). In contrast to rapamycin and PD0325901, other drugs including docetaxel, a standard-of-care chemotherapy for advanced prostate cancer (Pienta and Smith, 2005), were not predicted to be effective for inhibiting the FOXM1/CENPF regulon ($GRS_H = 5.8$ and $GRS_M = 5.6$; Figure 1B; Figure S1).

Systematic Inference of Drug Synergy

Next, we tested whether this computational approach could be extended to infer drug combinations that cooperate to inhibit MR activity, again using FOXM1 and CENPF as a proof of concept. These analyses are based on the hypothesis that effective drug combinations should induce a more significant reversal of MR-specific regulon expression, compared to the individual drugs (Figure 1C; Supplemental Experimental Procedures). Notably, such logic can be implemented based on individual drug signatures, without requiring in vivo signatures from drug combinations, which vastly increases the experimental efficiency for prioritizing drug combinations based on in vivo preclinical data.

To estimate a global synergistic reversion score (GSRS) for each drug pair, we assessed the predicted reversion score for all possible combinations of two drug treatments across each of the GEM models. First, the synergistic reversion score (SRS) was calculated for each GEM model as an harmonic mean

genes, thereby resulting in strong reversion. Scenario 2 illustrates two other drugs that inhibit (i.e., revert) relatively few target genes, thereby resulting in weak reversion.

(D) Heatmap representation depicting global synergistic reversion scores (GSRSs) for each possible pair of drugs across the series of GEM models based on FOXM1/CENPF human target genes. GSRSs were calculated by combining the synergistic reversion scores for targets affected by the drug combinations (see Supplemental Experimental Procedures). Heatmap intensity (blue) represents the predicted degree of reversion (GSRS); arrows indicate drug pairs with the highest combined GSRS.

(E) Heatmap showing the relative expression levels of FOXM1/CENPF target genes reverted by treatment with rapamycin or PD0325901 versus vehicle; also shown are genes that are not reverted (i.e., non-responsive) to these drugs.

Figure S1 is related to Figure 1; computational predictions of GRSs and GSRSs are provided in Tables S1 and S2, respectively.

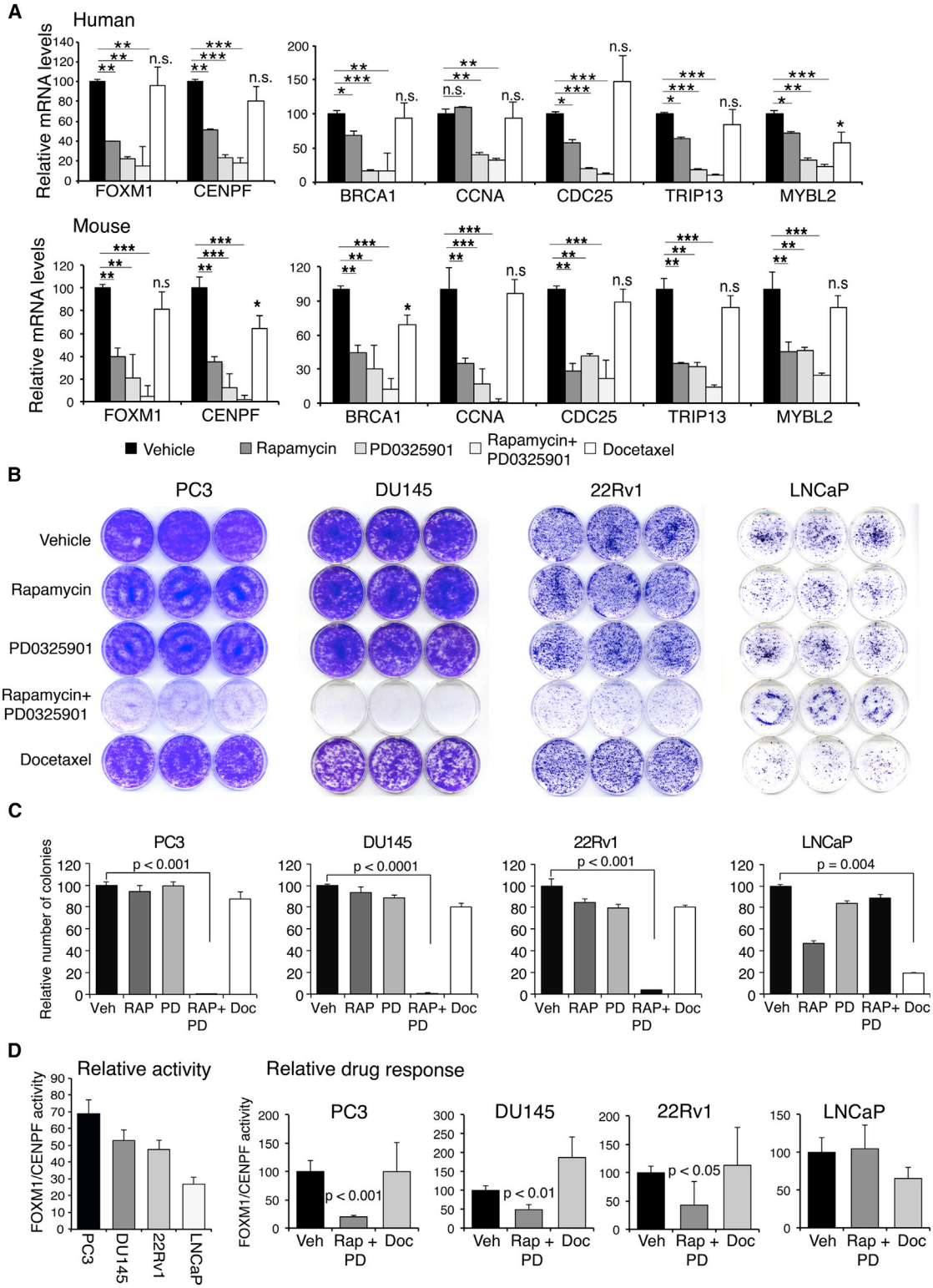

Figure 2. Validation of Drug Efficacy, Synergy, and Specificity in Prostate Cancer Cells

(A) Real-time PCR of mRNA expression levels of *FOXM1* and *CENPF* and their shared target genes following treatment with rapamycin and/or PD0325901 or docetaxel in DU145 human prostate cancer cells (top) or *NPK* mouse prostate tumors (bottom).

(B and C) Colony formation assays in the indicated human prostate cancer cells, PC3, DU145, 22Rv1, and LNCaP, following treatment with rapamycin (Rap) and/or PD0325901 (PD), or docetaxel (Doc). (B) Representative colony formation assays. (C) Quantification of independent assays performed in triplicate.

(legend continued on next page)

(F-score) that first maximizes the number of unique targets affected by each drug, and then the total number of targets affected by both drugs (Figure 1C; Supplemental Experimental Procedures). These analyses identified several combinations, most of which included rapamycin or PD0325901, which were predicted to be more effective than the individual compounds based on their GSRSs (Figure 1D; Table S2). In particular, the rapamycin + PD0325901 combination was predicted to have the strongest global inhibition of the FOXM1/CENPF regulon, both with respect to total number of targets affected by both drugs and the number of unique targets affected by each drug, resulting in the most significant negative global synergistic reversion score ($GSRS_H = -40.4$; p value < 0.001 compared to a random model; see Supplemental Experimental Procedures). This theoretical prediction was validated by assessment of FOXM1/CENPF target genes that were reverted by rapamycin or PD0325901 following drug treatment in vivo (Figure 1E).

Experimental Validation of Drug Specificity and Synergy in Cell Culture

Based on these computational predictions, we performed experimental validation to assess whether rapamycin and/or PD0325901 specifically inhibit the FOXM1/CENPF regulon in relevant mouse and human prostate cancer cell culture models, and if so, whether these drugs affect cell growth and tumorigenicity in a FOXM1/CENPF-dependent manner. First, we validated the underlying computational prediction that treatment with rapamycin and PD0325901 reverts the expression of shared target genes of FOXM1/CENPF. Using real-time PCR, we found that treatment with rapamycin and PD0325901, but not docetaxel, inhibited expression of both FOXM1 and CENPF as well as their shared target genes in several human and mouse prostate cancer models (Figure 2A; Figure S2A). This inhibition of target genes was coincident with inhibition of the corresponding signaling pathways, namely PI3K/mTOR and MAP kinase in the mouse and human cells (Figures S2B and S2C). Notably, inhibition of colony formation was significantly greater when the drugs were combined than when used individually (Figure 2B, C), which supports the computational prediction of rapamycin + PD0325901 synergy.

To address the specificity of the rapamycin + PD0325901 drug combination for inhibition of FOXM1/CENPF activity, we assessed whether this combination was preferentially more potent in contexts having high levels of FOXM1/CENPF activity. First, we surveyed the expression and activity of FOXM1/CENPF in a series of human and mouse cell lines; "activity" was determined experimentally by analyses of the expression of FOXM1/CENPF shared target genes (Figure 2D; Figures S2D–S2F). These studies revealed that PC3 cells have the highest levels of FOXM1/CENPF activity, whereas LNCaP cells have lower levels (Figure 2D). Correspondingly, human prostate cancer cells with higher levels of FOXM1/CENPF activity had greater response to rapamycin + PD0325901 treatment, as evident from the strong inhibition of activity and colony formation, whereas LNCaP cells, which have low levels of FOXM1/CENPF activity, had a modest response to rapamycin + PD0325901 (Figures 2B–2D). In contrast, this relationship to FOXM1/CENPF activity was not observed following docetaxel treatment of these cells (Figures 2B–2D). Similar findings were observed in mouse prostate cancer cells wherein response to rapamycin + PD0325901 treatment was correlated with the relative levels of FoxM1/Cenpf activity (Figures S2D and S2E).

Moreover, the dependence on FOXM1/CENPF in the human prostate cancer cells was evident by the reduction in the half maximal inhibitory concentration (IC_{50}) for rapamycin + PD0325901, but not docetaxel, following the silencing of both FOXM1 and CENPF in human prostate cancer cell lines with high levels of activity (Figure S3). Conversely, overexpression of FOXM1 and CENPF in a non-prostate cancer cell line, HEK293, resulted in an increase in the IC_{50} for rapamycin + PD0325901, but not docetaxel (Figure S3). Taken together, these findings validate the computational prediction that FOXM1/CENPF activity is specifically inhibited by rapamycin + PD0325901.

Experimental Validation of Drug Efficacy and Specificity In Vivo

The synergistic effects of combined treatment with rapamycin + PD0325901 were even more dramatic in vivo. In particular, we performed preclinical studies using *NPK* mice (*Nkx3.1*^{CreERt2}; *Pten*$^{flox/flox}$; *Kras*$^{LSL\text{-}G12D/+}$), which model aggressive, metastatic prostate cancer that is dependent on FOXM1/CENPF activity (Aytes et al., 2013, 2014). Tumor-bearing *NPK* mice were treated with rapamycin and/or PD0325901, or docetaxel, for 5 days (i.e., the dynamic response cohort) or 1 month (i.e., the therapeutic response cohort) (Figure 3A; Table S3). Mice were then either sacrificed for analysis or monitored for the effects of drug treatment on survival and metastasis (i.e., the survival response cohort) (Figure 3A; Table S3).

Whereas treatment with either drug individually had a modest therapeutic benefit at the various endpoints, the combination of rapamycin + PD0325901 had a profound effect at all tumor endpoints in the therapeutic response cohort (Figures 3B–3E). In particular, treatment with rapamycin + PD0325901, but not docetaxel, resulted in profound abrogation of the histological phenotype, coincident with inhibition of relevant signaling pathways, as evident by immunohistochemistry (Figure 3B). Moreover, tumors treated with rapamycin + PD0325901, but not docetaxel, displayed a significant decrease in cellular proliferation (p < 0.0001) (Figure 3C), as well as significant reduction in tumor burden, as measured by tumor weight (p = 0.003) and tumor volume using MRI (p < 0.01) (Figures 3D and 3E). Furthermore, these effects on phenotype and tumor burden were accompanied by a significant improvement in survival (p < 0.0001) (Figure 3F), as well as a 3-fold reduction in the incidence of

(D) (Left) Relative activity of FOXM1/CENPF in human prostate cancer cells lines. Activity levels were calculated based on expression levels of 10 FOXM1/CENPF target genes (see Figure S2F). (Right) Relative drug response assessed for FOXM1/CENPF activity levels in the human prostate cancer cell lines following treatment with rapamycin + PD0325901 (Rap + PD) or docetaxel (Doc). Differences between treatment groups were assessed using Student's t test. When indicated, p values are represented as *p < 0.01, **p < 0.001, and ***p < 0.0001. Bars represent mean ± SD.
Figures S2 and S3 are related to Figure 2.

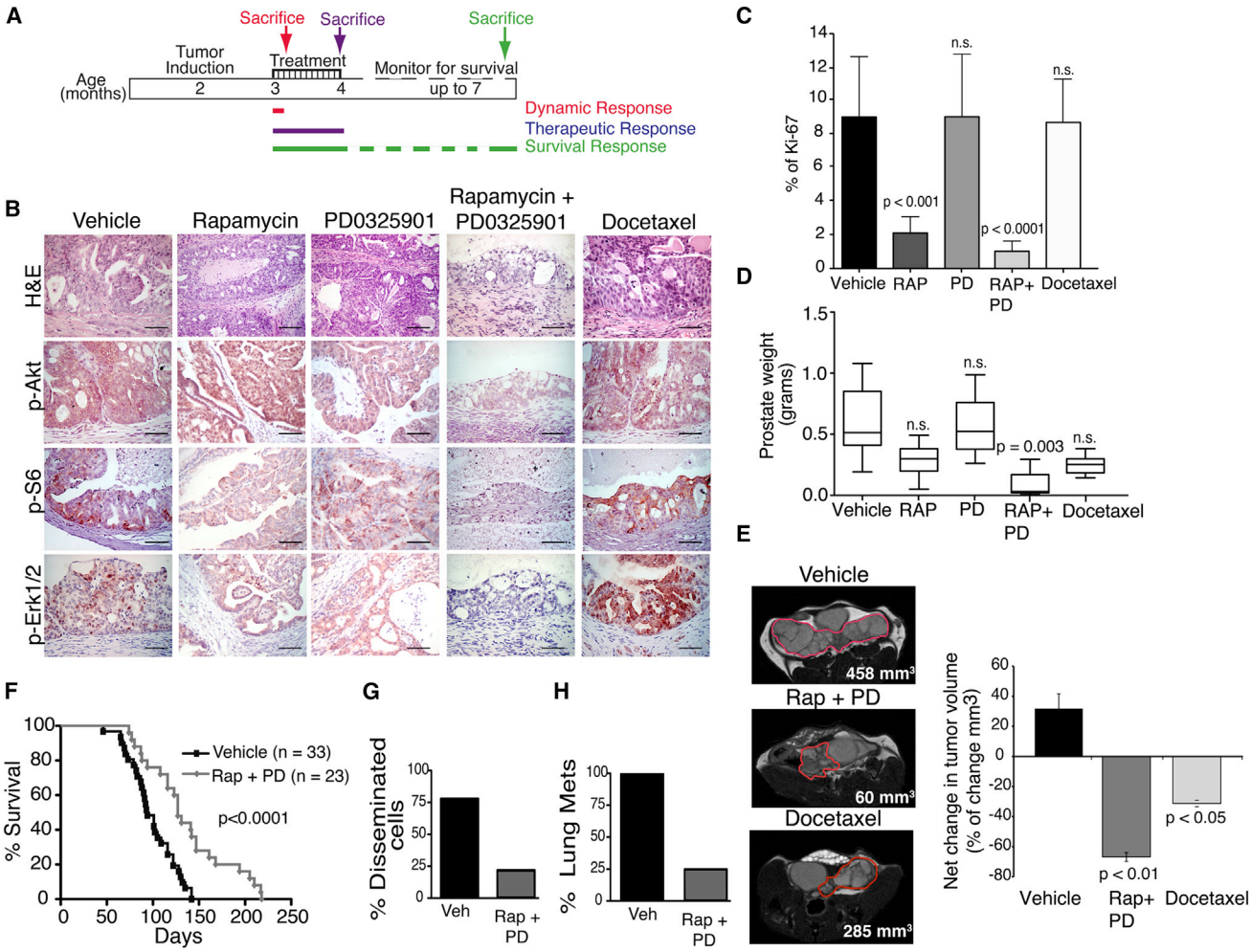

Figure 3. Validation of Drug Synergy and Specificity In Vivo

(A) Shown is the design of preclinical studies. *NPK* mice were induced to form tumors by delivery of tamoxifen at 2 months of age as in (Aytes et al., 2013). Mice were treated with rapamycin and/or PD032590, or docetaxel for 5 days (dynamic response cohort) or 1 month, following which mice were sacrificed for analyses (therapeutic response cohort) or monitored for survival (survival response cohort).

(B–E) Analysis of the therapeutic response cohort following treatment with rapamycin (Rap) and/or PD0325901 (PD) or docetaxel (Doc) as indicated (n = 5 mice/treatment group). (B) Representative sections of H&E staining or immunohistochemical staining for the indicated markers of the PI3K/mTOR or MAP kinase signaling pathways; scale bars represent 100 μm. (C) Relative cellular proliferation following drug treatment as determined by the percent of Ki67-positive cells relative to total epithelial cells. (D) Prostate weight (in grams) following drug treatment. (E) Longitudinal MRI imaging showing representative images following drug treatment with tumor volumes indicated. The panel to the right represents the net change in tumor volume following 1 month of drug treatment.

(F–H) Shown is analysis of the survival response cohort. (F) Survival analysis showing the improvement in survival following treatment with rapamycin and PD0325901 (Rap + PD) compared with the vehicle-treated mice. (G) Percentage of mice with disseminated cells in the bone marrow and (H) percentage of mice with lung metastases following treatment with vehicle (Veh) or rapamycin + PD0325901 (Rap + PD) (n = 10 mice/treatment group). Differences between groups were assessed using Student's t test; bars represent mean ± SD. In (F), p value corresponds to a log-rank test.

disseminated tumor cells in the bone marrow and a 4-fold reduction in the incidence of lung metastases (Figures 3G and 3H). Together, these findings validate the concept that treatment with rapamycin + PD0325901 inhibits growth of FOXM1/CENPF-dependent tumors.

Relationship of Mouse Drug-Treatment Signatures to Human Cancer

Given the striking reduction in tumor and metastatic burden following treatment with rapamycin + PD0325901, we evaluated whether this combination might be sufficient to broadly inhibit molecular processes associated with advanced, FOXM1/CENPF-dependent prostate cancer. We addressed this question by analyzing signatures obtained by differential gene expression analysis of *NPK* prostate tumors treated with vehicle or rapamycin + PD0325901 for 1 month (i.e., the therapeutic response cohort; Table S3), which resulted in extensive abrogation of the tumor phenotype (see Figure 3). We compared this "therapeutic response" signature to a reference mouse "tumor" signature, corresponding to differential gene expression

between phenotypically wild-type prostates and *NPK* prostate tumors, which captures the transition from normal prostate to fully malignant prostate cancer (Table S3). Strikingly, genes that were differentially expressed in the therapeutic response signature were strongly negatively enriched in the mouse tumor signature (NES = −8.58; $p < 0.001$) (Figure S4A). Further evidence that rapamycin + PD0325901 treatment results in broad inhibition beyond their respective target signaling pathways was provided by biological pathway analysis. In particular, pathways that were significantly inhibited (i.e., reverted) following treatment of the *NPK* tumors with rapamycin + PD0325901, but not docetaxel, include several that are important for tumor progression and are not directly related to mTOR/PI3K/MAP kinase signaling (Figure 4A; Table S4).

To evaluate molecular processes that are inhibited immediately following drug treatment, we analyzed a "dynamic response" signature, representing a time point wherein the drugs are active but the tumor phenotype has not yet been abrogated (Figure 3A; Table S3; and data not shown). In particular, this short-term treatment with rapamycin + PD0325901 resulted in reversion of FOXM1/CENPF targets, as predicted by our computational approach (Figure S4B; see Figure 1E). Comparison of this "dynamic response" signature to a reference mouse "malignancy signature," based on comparison of non-malignant prostate tumors from *NP* mice to fully malignant *NPK* tumors (Aytes et al., 2013), revealed a striking negative enrichment (i.e., strong reversion) (NES = −8.34; $p < 0.001$) (Figure 4B), suggesting that the rapamycin + PD0325901 combination inhibits molecular processes associated with *NPK* tumor malignancy even prior to their overt effects on the tumor phenotype.

To assess conservation of these molecular changes with human prostate cancer, we performed GSEA to compare a humanized version of the mouse dynamic response signature with human prostate cancer signatures (see Supplemental Experimental Procedures). We used three independent human prostate cancer signatures, each of which is based on distinct clinical endpoints (Table S3): (1) a malignancy signature based on the Taylor dataset (Taylor et al., 2010), which compares patients having low Gleason score and no biochemical recurrence ($n = 39$) to those with high Gleason score and a short time to biochemical recurrence ($n = 10$) (Aytes et al., 2013); (2) a metastasis signature based on the Balk dataset (Stanbrough et al., 2006), which compares hormone-naive prostate tumors ($n = 22$) to bone metastases from castration-resistant prostate cancer ($n = 29$) (Aytes et al., 2014); and (3) a survival signature based on the Sboner dataset (Sboner et al., 2010), which compares transurethral resections from patients who survived for nearly 200 months ($n = 12$) to those who died of prostate cancer within 12 months ($n = 6$) (Wang et al., 2013). Strikingly, the mouse dynamic response signature was strongly negatively enriched when compared with each of these human signatures, indicating that genes that are consistently overexpressed in aggressive prostate cancer are inhibited following drug treatment (Taylor signature NES = −5.48, $p < 0.001$; Balk signature NES = −5.26, $p < 0.001$; and Sboner signature NES = −6.40, $p < 0.001$) (Figure 4C). In contrast, the docetaxel treatment response signature was either minimally or not negatively enriched in these human signatures (Figure S4C).

We then asked whether the mouse dynamic response signature could reverse a "FOXM1/CENPF activity" signature in human prostate cancer. This FOXM1/CENPF activity signature, defined using the Sboner dataset (Sboner et al., 2010), corresponds to differential gene expression between patient samples having low versus high levels of FOXM1/CENPF activity, which was measured by enrichment of the FOXM1/CENPF regulon in each patient using single-sample master regulator inference algorithm (ssMARINa) as in Aytes et al. (2014) (see Supplemental Experimental Procedures). GSEA comparing the "FOXM1/CENPF" activity signature with the mouse "dynamic response" signature showed strong negative enrichment (NES = −6.43, $p < 0.001$) (Figure 4D), which supports the concept that patients with high levels of FOXM1/CENPF activity should respond more effectively to rapamycin + PD0325901 treatment. Notably, similar comparison with a docetaxel treatment response signature did not indicate such relationship (NES = 0.37, $p = 0.77$) (Figure S4D).

We further evaluated the correlation between FOXM1/CENPF activity levels and predicted treatment response in each patient in the Sboner dataset estimated using ssMARINa and GSEA, respectively. We found that inferred FOXM1/CENPF activity levels and predicted treatment response were strongly correlated (Spearman's rho = 0.51, $p < 2.2 \times 10^{-16}$) (Figure 4E), which was not the case for the docetaxel treatment response (Figure S4E). Taken together, these computational analyses suggest that the molecular programs (i.e., genes and pathways) specifically inhibited (reverted) by rapamycin + PD0325901 in the mouse model are conserved with those that drive aggressive human prostate cancer, and in particular in patients having high levels of FOXM1/CENPF activity.

Conservation of Treatment Response in Mouse and Human Prostate Cancer

Given the conservation in the molecular programs affected by drug treatment in the GEM models and human prostate cancer, we next asked whether we could use the mouse treatment response signature to identify genes predicted to be associated with treatment response in humans. First, we identified candidate rapamycin + PD0325901-responsive genes by interrogating the mouse prostate cancer interactome (Aytes et al., 2014) with the dynamic response signature using the standard MARINa algorithm to identify MRs of treatment response in the mouse (Lefebvre et al., 2010). We then compared these MRs with the orthologous human genes to identify those predicted both to be regulated by FOXM1/CENPF in human prostate cancer and to be downregulated by drug treatment; we refer to these as "predicted treatment-responsive genes" and distinguish them from other FOXM1/CENPF target genes that are not predicted to be responsive to the treatment (Figure 5A). Notably, real-time PCR analyses confirmed that the expression levels of these predicted treatment-responsive genes were indeed inhibited by rapamycin + PD0325901 in human prostate cancer cell lines, whereas the expression levels of the predicted non-responsive genes were not inhibited by such treatment (Figure 5B).

These treatment-responsive genes (including *TOP2A*, *UHRF1*, *ASF1B*, *MCM4*, *WHSC1*, *MCM2*, *SUV39H1*, *BLM*, *BRCA1*,

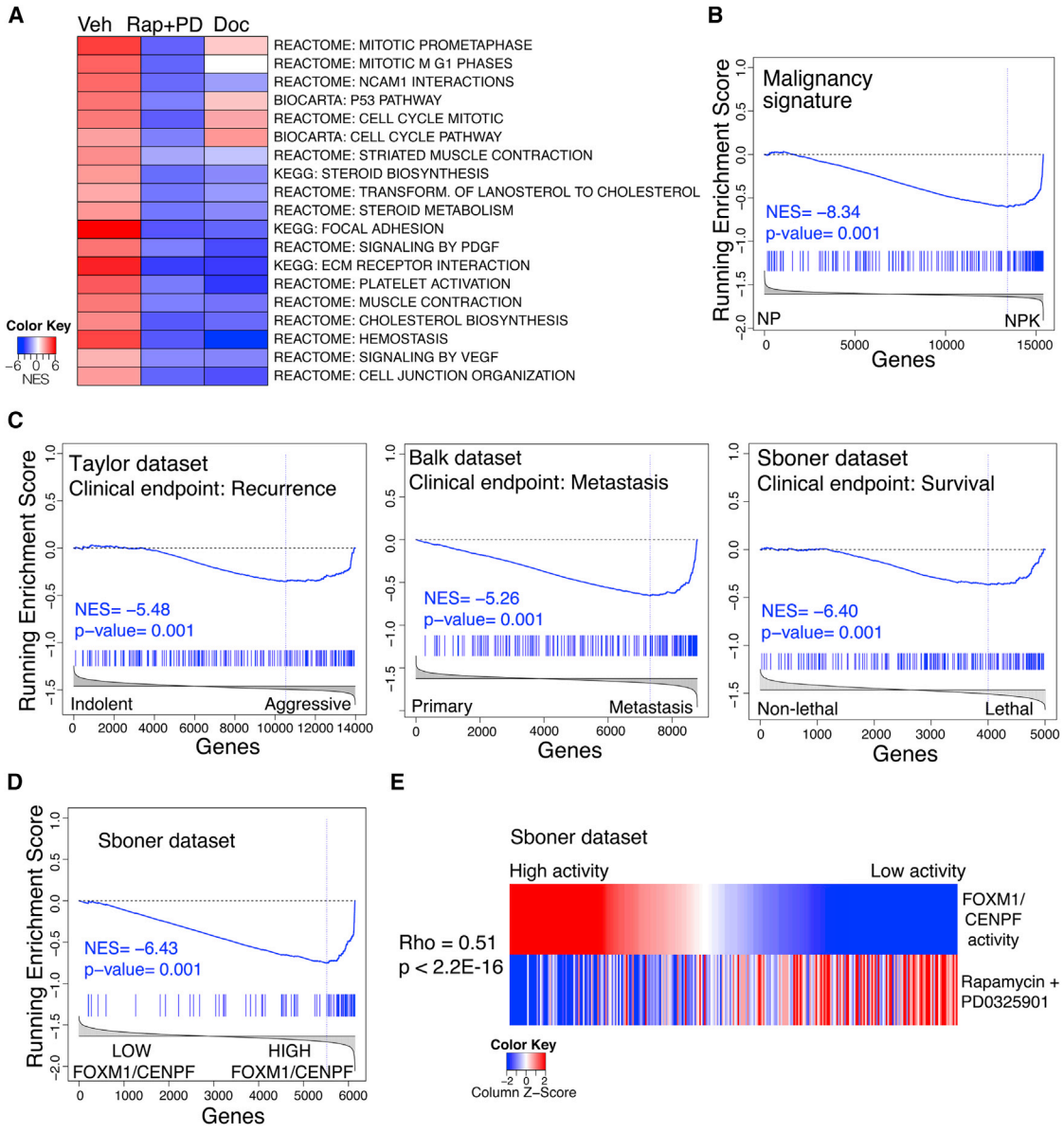

Figure 4. Cross-Species Analyses of Drug-Treatment Response

(A) Heatmap depiction showing representative pathways that are significantly changed following treatment with rapamycin + PD0325901 (Rap + PD) or docetaxel (Doc) relative to vehicle treatment (Veh). Pathway analysis was done by GSEA using a "humanized" version of the dynamic response allograft tumor signature (see Table S3 and Supplemental Experimental Procedures). A complete list of pathways is provided in Table S4.

(B–D) GSEA using as the query gene set the mouse rapamycin + PD0325901 dynamic treatment response signature (B) or a "humanized" version of this signature (C and D); normalized enrichment score (NES) and associated p values are shown. In (B), the reference is mouse "malignancy" signature, which represents differentially expressed genes from *NP* versus *NPK* mouse tumors as reported previously (Aytes et al., 2013). In (C), the references are three independent human tumor signatures (i.e., Taylor, Balk, or Sboner), each of which compare differentially expressed genes representing less aggressive versus more aggressive prostate cancer specimens (Table S3). In (D), the reference signature represents differentially expressed genes in patients from the Sboner dataset having low versus high levels of FOXM1/CENPF activity, which was inferred using single sample MARINa (ssMARINa) (see Supplemental Experimental Procedures).

(E) Heatmap showing the correlation in human patients from the Sboner dataset of FOXM1/CENPF activity levels (top) with the corresponding predicted drug-treatment response for rapamycin + PD0325901 (bottom). As above, FOXM1/CENPF activity was estimated for each patient using ssMARINa. The treatment response for each patient was inferred using a "humanized" version of the mouse dynamic treatment signature using GSEA (see Supplemental Experimental Procedures). Correlation coefficient (rho) and associated p value were estimated using Spearman's correlation.

Figure S4 and Tables S3 and S4 are related to Figure 4.

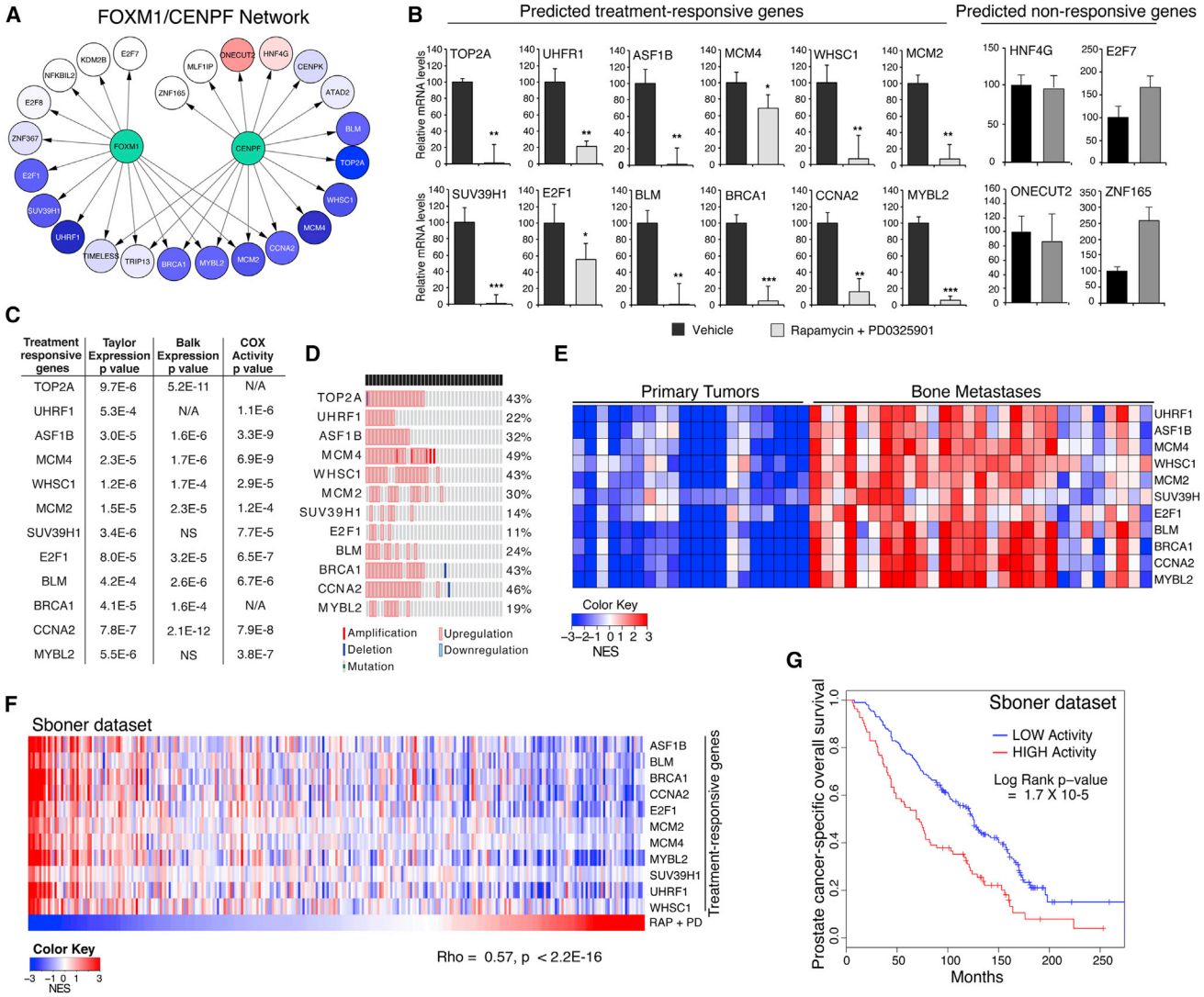

Figure 5. Conservation of Treatment Responsive Genes in Human Prostate Cancer

(A) FOXM1/CENPF subnetwork of human target genes predicted to be responsive or non-responsive to treatment with rapamycin + PD0325901 based on comparison with treatment response for the mouse model. Relative change in activity following drug treatment is indicated by levels of "blue" for genes predicted to be reverted by the drugs and levels of "red" for those predicted to be activated or unaffected (i.e., non-responsive).

(B) Real-time PCR showing the actual change in expression levels of FOXM1/CENPF target genes following treatment with vehicle or rapamycin + PD0325901. The "predicted treatment-responsive genes" correspond to those represented by the blue circles in (A), and the "predicted non-responsive genes" to the other genes. PCR was done using DU145 cells; differences were assessed using t test (p values are represented as *$p < 0.01$, **$p < 0.001$, and ***$p < 0.0001$) and bars represent mean ± SD.

(C–E) Association of predicted treatment-responsive genes with lethal prostate cancer and disease outcome. (C) Summary table showing the significance of elevated expression levels in metastases versus primary tumors in the Taylor and Balk datasets (columns on the left; p value was calculated using t test). The column on the right shows a COX regression model indicating the association based on master regulator activity levels of the predicted treatment-responsive genes with prostate cancer-specific survival estimated for patients in the Sboner dataset; COX p value was calculated using Wald test (NA, sufficient targets not represented; NS, not significant). (D) Oncoprint visualization from cBioportal showing the percent of alterations of the predicted treatment-responsive genes in metastases samples from the Taylor dataset. (E) Heatmap showing the master regulator activity levels of treatment-responsive genes in primary tumors versus bone metastases from the Balk dataset.

(F) Heatmap comparing the master regulator activity levels of the treatment-responsive genes (upper rows) across each patient in the Sboner dataset with inferred treatment response for each patient (Rap +PD, bottom row). The activity levels and the treatment response for each patient were estimated using single-sample MARINa (ssMARINa) and GSEA, respectively (see Supplemental Experimental Procedures). The correlation between the average activity levels of all treatment-responsive genes and the predicted response was estimated using Spearman's correlation.

(G) Kaplan-Meier survival analysis based on the master regulator activity levels of predicted treatment-responsive genes in the Sboner dataset using prostate cancer-specific survival as the endpoint. The p value was estimated using a log-rank test of the difference in outcome between patients with higher activity levels (red) and those with lower/no activity (blue).

CCNA2, *E2F1*, and *MYBL2*) have known functions in DNA repair, epigenetic modifications, cell cycle, proliferation, and/or survival, which are all associated with cancer malignancy. Notably, each of these is overexpressed in advanced human prostate cancer, and their activity levels are associated with disease outcome, as shown by univariate analyses using a COX proportional hazard model on the Sboner dataset (Figures 5C and 5D). Moreover, analyses based on the Balk dataset revealed robust activity levels of the treatment-responsive genes in metastatic samples compared to primary tumors (Figure 5E).

We further demonstrated the association of the activity levels of the treatment-responsive genes with drug response on a patient-by-patient basis, estimated using ssMARINa and GSEA, respectively, on the Sboner dataset (Figure 5F). In particular, the average activity levels of treatment-responsive genes were strikingly correlated with the rapamycin + PD0325901 drug response (Spearman rho = 0.57, $p < 2.2 \times 10^{-16}$) (Figure 5F), similar to that observed for the FOXM1/CENPF activity (see Figure 4D). Most notably, multivariate Kaplan-Meier survival analysis on the Sboner dataset to evaluate disease-specific survival revealed that patients with higher activity levels of the treatment-responsive genes have a shorter time to prostate cancer-specific death compared to patients with lower activity levels (log-rank p value = 1.7×10^{-5}) (Figure 5G). Importantly, the activity of the treatment-responsive subnetwork of the FOXM1/CENPF regulon was more significant than the FOXM1/CENPF regulon (log-rank p value = 1.3×10^{-4}) and also outperformed a random comparable set of genes with respect to the COX proportional hazard model (p value for improvement < 0.001) and Kaplan-Meier survival analysis (p value for improvement < 0.015) (see Supplemental Experimental Procedures). Taken together, these findings suggest that computationally predicted treatment-responsive genes can be used to identify patients that are likely to benefit from treatment with drugs that co-target the PI3K/mTOR and MAP kinase signaling pathways and provide a proof of concept for the overall approach.

DISCUSSION

In this study, we introduce a generalizable computational approach to extrapolate in vivo preclinical treatment data from GEM models to inform on human cancer treatment. Our method infers drug efficacy based on the ability of a given drug to revert the transcriptional regulon of key dependencies that drive the tumor phenotype. Importantly, we show that this method can be used to prioritize drug combinations based on analysis of individual compounds, which greatly enhances the value of in vivo preclinical analyses of compounds in mice. We demonstrate this approach with a proof-of-concept study based on identification of drugs and drug combinations that inhibit the activity of FOXM1/CENPF, which were chosen for their established relevance for lethal prostate cancer (Aytes et al., 2014). However, this approach should be applicable to identify candidate drugs and drug combinations for many other driver gene(s) of interest and not limited to prostate cancer. Notably, the molecular programs affected by drug treatment in the GEM model are well conserved with human prostate cancer, which supports the concept that analyses of drug-treatment data from mouse models can be used to identify treatment-responsive genes for human prostate cancer. Thus, we have described a method to identify drugs and drug combinations that specifically inhibit cancer driver genes, as well as to identify potential biomarkers to predict the efficacy of drug treatments for individual patients.

Several features of our approach distinguish it from other strategies previously used to screen for drug response in human cancer. First, most other approaches have been based on analyses of cancer cell lines in culture (e.g., Barretina et al., 2012; Garnett et al., 2012), whereas our study is based on drug perturbation of GEM models in vivo. Thus, we evaluate drug efficacy in the context of the native tumor microenvironment and intact immune system, which are now widely recognized as being essential for drug response in vivo, particularly given recent advances in immunotherapy. Although the tumor context of any individual GEM model is unlikely to fully recapitulate that of human cancer, we address this limitation by analyzing multiple distinct GEM models to avoid idiosyncratic GEM-specific biology. Indeed, we have observed a remarkable concordance of the molecular consequences of drug treatment between our "consensus" analyses of mouse models and human prostate cancer.

A second distinguishing feature of our approach is its ability to identify synergistic drug combinations based on single-agent treatment data. From a practical standpoint, the number of drugs that can be feasibly evaluated using in vivo perturbations in a series of GEM models is limited. Therefore, the ability to evaluate the efficacy of drug combinations by profiling a relatively small number of single drugs (e.g., the 100 most relevant compounds) would allow assessment of a very large potential combination therapy space (e.g., 4,950 combinations), thus affording significant economy of scale.

A third important feature is that our computational method identifies drugs based on their ability to inhibit specific drivers of the tumor phenotype, rather than on overall toxicity or inhibition of more general tumor-related parameters. In particular, the method evaluates the efficacy of drug response based on inhibition of the transcriptional regulon of specific master regulators of interest. Furthermore, our computational analysis of treatment response in the GEM models in vivo has also identified treatment-responsive genes that are conserved in human prostate cancer. We propose that such treatment-responsive genes may serve as surrogate biomarkers to infer the potential efficacy of drug treatments in patients. In particular, our current findings suggest that previous analyses may have underestimated the value of molecular inference of preclinical data from GEM models for not only predicting optimal drug combinations but also identifying molecular markers for predicting treatment response to such drugs.

The PI3K/mTOR and MAP kinase signaling pathways are known to be dysregulated in many advanced prostate cancers (Aytes et al., 2013; Kinkade et al., 2008; Taylor et al., 2010). Currently, drugs that target these pathways (albeit not rapamycin and PD0325901) are being evaluated in numerous clinical trials for prostate cancer and many other solid tumors, including combination-therapy regimes. Results from the current study as well as previous work (Aytes et al., 2014) suggest that aberrant levels of FOXM1 and CENPF, as assessed by immunostaining of tumor samples, may identify patients who would likely benefit from

treatment with agents that target the PI3K/mTOR and/or MAP kinase signaling pathways. In addition, our study suggests that the treatment-responsive genes we have identified could provide intermediate biomarkers to assess short-term efficacy of combination therapy in patients, a strategy that can be readily generalized to other targets and therapies. Thus, our studies may inform or modulate the design of clinical trials or help provide a mechanistic basis for clinical findings.

Beyond prostate cancer, our computational methodology may be beneficial to identify drugs that target key actionable targets in vivo for a wide range of tumor types, oncogene and non-oncogene dependencies, and therapeutic agents, including both US Food and Drug Administration-approved and experimental compounds. Since many cancer types now have relevant GEM models that are being used in many preclinical studies, it would be advantageous to use our approach to apply these preclinical data from GEMs to analyze treatment response in human cancer.

EXPERIMENTAL PROCEDURES

Computational Prediction of Drug Synergy

Computational inference of drugs that inhibit FOXM1 and CENPF activity was done using their shared target genes predicted from the mouse or human prostate cancer interactomes and using in vivo drug perturbation data, which were described previously (Aytes et al., 2014). Target gene reversion (i.e., inhibition) was assessed using GSEA for each drug across each GEM model. GRSs for each drug were then inferred by integrating the reversion scores across each GEM model using a metric based on the Stouffer integration formulation (Whitlock, 2005). Optimal drug combinations were predicted from the single-agent in vivo drug perturbation data by determining the SRSs for each drug using an harmonic mean (F1 statistical measure), which maximizes the number of unique targets affected by each drug as well as the total number of targets affected by two drugs. GSRSs were then estimated as an average SRS weighted by the number of mouse models in which a drug pair was estimated to be effective (i.e., to share a non-zero SRS). Details of the computational methods used to compute GRSs and GSRSs are provided in Supplemental Experimental Procedures, and the data are provided in Tables S1 and S2.

Efficacy of Drug Treatment

All experiments using animals were performed according to protocols approved by the Institutional Animal Care and Use Committee at Columbia University Medical Center. Cell culture studies were done as described previously (Aytes et al., 2014) using human prostate cancer cell lines obtained from ATCC and mouse cell lines derived from the GEM models used herein (Aytes et al., 2013; unpublished date). Rapamycin and docetaxel were purchased from LC Laboratories, and PD0325901 was provided by Pfizer. Cell culture assays were performed in a minimum of two independent experiments each done in triplicate; data are presented by the mean ± SD. For in vivo studies, tumor-bearing *NPK* mice (Aytes et al., 2013) or allografted *NPK* tumors were treated with vehicle or rapamycin (10 mg/kg) and/or PD0325901 (10 mg/kg) or docetaxel (10 mg/kg) as described previously (Kinkade et al., 2008). At the time of sacrifice, tissues were collected for histopathological and molecular analysis as described elsewhere (Aytes et al., 2013; Kinkade et al., 2008). GraphPad Prism software (version 5.0) was used for statistical analyses and to generate data plots. A complete list of primers used in this study is provided in Table S5.

Cross-Species Computational Analysis of Drug-Treatment Signatures

Gene expression profiles based on Illumina expression arrays as in Aytes et al. (2014) were used to generate drug-treatment signatures for the mouse tumors or allografts, as detailed in Table S3. For comparison of mouse treatment signatures with human signatures, the mouse genes were mapped to their corresponding human orthologs. Single-sample computation of FOXM1/CENPF activity levels or drug treatment across human patients was inferred for each patient sample using single-sample MaRINA (ssMARINa) and GSEA, respectively (Aytes et al., 2014) (see Supplemental Experimental Procedures). COX proportional hazard model and Kaplan-Meier analysis were done using the "surv" and "coxph" functions from the survcomp package in R v2.14.0.

ACCESSION NUMBERS

The accession numbers for the gene expression profiling data reported in this study are GEO: GSE69211 and GEO: GSE69213.

SUPPLEMENTAL INFORMATION

Supplemental Information includes Supplemental Experimental Procedures, four figures, and five tables and can be found with this article online at http://dx.doi.org/10.1016/j.celrep.2015.08.051.

AUTHOR CONTRIBUTIONS

A.M. performed all of the computational analyses, and A.A. performed all of the experimental analyses. M.Z. provided the new mouse cell lines described herein. A.M., A.A., M.M.S., C.A.-S., and A.C. designed experiments, analyzed the data, and wrote the paper.

CONFLICTS OF INTEREST

A.C. is a founder and stockholder of Darwin Health and Therasis and a consultant for Dow AgroSciences, Thermo Fisher Scientific, and Cancer Genetics Inc.

ACKNOWLEDGMENTS

This work was supported by grants CA173481 (to C.A.-S.), U01 CA084294 (to C.A.-S., M.M.S., and A.C.), U54 CA121852 (to A.C., C.A.-S., M.M.S.), P01 CA154293 (to M.M.S. and C.A.-S.), U01HL111566-02S2 (to A.C.) and U01CA168426 (to A.C.). A.A. was a recipient of a Marie Curie International Outgoing Fellowship (PIOF-GA-2009-253290), co-sponsored with the Catalan Institute of Oncology-Bellvitge Institute for Biomedical Research, Barcelona, Spain, and a recipient of a pilot award from the Irving Institute for Clinical and Translational Research at Columbia University supported by the National Center for Advancing Translational Sciences, NIH (UL1 TR000040). A.M. is a recipient of a Prostate Cancer Foundation Young Investigator Award. C.A.-S. is an American Cancer Society Research Professor supported in part by a generous gift from the F.M. Kirby Foundation.

Received: December 16, 2014
Revised: June 2, 2015
Accepted: August 17, 2015
Published: September 17, 2015

REFERENCES

Abate-Shen, C., and Pandolfi, P.P. (2013). Effective utilization and appropriate selection of genetically engineered mouse models for translational integration of mouse and human trials. Cold Spring Harb. Protoc. *2013*, 2013.

Al-Lazikani, B., Banerji, U., and Workman, P. (2012). Combinatorial drug therapy for cancer in the post-genomic era. Nat. Biotechnol. *30*, 679–692.

Aytes, A., Mitrofanova, A., Kinkade, C.W., Lefebvre, C., Lei, M., Phelan, V., LeKaye, H.C., Koutcher, J.A., Cardiff, R.D., Califano, A., et al. (2013). ETV4 promotes metastasis in response to activation of PI3-kinase and Ras signaling in a mouse model of advanced prostate cancer. Proc. Natl. Acad. Sci. USA *110*, E3506–E3515.

Aytes, A., Mitrofanova, A., Lefebvre, C., Alvarez, M.J., Castillo-Martin, M., Zheng, T., Eastham, J.A., Gopalan, A., Pienta, K.J., Shen, M.M., et al.

(2014). Cross-species regulatory network analysis identifies a synergistic interaction between FOXM1 and CENPF that drives prostate cancer malignancy. Cancer Cell *25*, 638–651.

Barretina, J., Caponigro, G., Stransky, N., Venkatesan, K., Margolin, A.A., Kim, S., Wilson, C.J., Lehár, J., Kryukov, G.V., Sonkin, D., et al. (2012). The Cancer Cell Line Encyclopedia enables predictive modelling of anticancer drug sensitivity. Nature *483*, 603–607.

Carro, M.S., Lim, W.K., Alvarez, M.J., Bollo, R.J., Zhao, X., Snyder, E.Y., Sulman, E.P., Anne, S.L., Doetsch, F., Colman, H., et al. (2010). The transcriptional network for mesenchymal transformation of brain tumours. Nature *463*, 318–325.

Chang, A.J., Autio, K.A., Roach, M., 3rd, and Scher, H.I. (2014). High-risk prostate cancer-classification and therapy. Nat. Rev. Clin. Oncol. *11*, 308–323.

Chen, J.C., Alvarez, M.J., Talos, F., Dhruv, H., Rieckhof, G.E., Iyer, A., Diefes, K.L., Aldape, K., Berens, M., Shen, M.M., and Califano, A. (2014). Identification of causal genetic drivers of human disease through systems-level analysis of regulatory networks. Cell *159*, 402–414.

Cooperberg, M.R., Moul, J.W., and Carroll, P.R. (2005). The changing face of prostate cancer. J. Clin. Oncol. *23*, 8146–8151.

Garnett, M.J., Edelman, E.J., Heidorn, S.J., Greenman, C.D., Dastur, A., Lau, K.W., Greninger, P., Thompson, I.R., Luo, X., Soares, J., et al. (2012). Systematic identification of genomic markers of drug sensitivity in cancer cells. Nature *483*, 570–575.

Garraway, L.A., and Lander, E.S. (2013). Lessons from the cancer genome. Cell *153*, 17–37.

Kinkade, C.W., Castillo-Martin, M., Puzio-Kuter, A., Yan, J., Foster, T.H., Gao, H., Sun, Y., Ouyang, X., Gerald, W.L., Cordon-Cardo, C., and Abate-Shen, C. (2008). Targeting AKT/mTOR and ERK MAPK signaling inhibits hormone-refractory prostate cancer in a preclinical mouse model. J. Clin. Invest. *118*, 3051–3064.

Lefebvre, C., Rajbhandari, P., Alvarez, M.J., Bandaru, P., Lim, W.K., Sato, M., Wang, K., Sumazin, P., Kustagi, M., Bisikirska, B.C., et al. (2010). A human B-cell interactome identifies MYB and FOXM1 as master regulators of proliferation in germinal centers. Mol. Syst. Biol. *6*, 377.

Luo, J., Solimini, N.L., and Elledge, S.J. (2009). Principles of cancer therapy: oncogene and non-oncogene addiction. Cell *136*, 823–837.

Mukherji, D., Omlin, A., Pezaro, C., Shamseddine, A., and de Bono, J. (2014). Metastatic castration-resistant prostate cancer (CRPC): preclinical and clinical evidence for the sequential use of novel therapeutics. Cancer Metastasis Rev. *33*, 555–566.

Pienta, K.J., and Smith, D.C. (2005). Advances in prostate cancer chemotherapy: a new era begins. CA Cancer J Clin *55*, 300–318, quiz 323-305.

Politi, K., and Pao, W. (2011). How genetically engineered mouse tumor models provide insights into human cancers. J. Clin. Oncol. *29*, 2273–2281.

Rathkopf, D., and Scher, H.I. (2013). Androgen receptor antagonists in castration-resistant prostate cancer. Cancer J. *19*, 43–49.

Roychowdhury, S., and Chinnaiyan, A.M. (2013). Advancing precision medicine for prostate cancer through genomics. J. Clin. Oncol. *31*, 1866–1873.

Rubio-Perez, C., Tamborero, D., Schroeder, M.P., Antolín, A.A., Deu-Pons, J., Perez-Llamas, C., Mestres, J., Gonzalez-Perez, A., and Lopez-Bigas, N. (2015). In silico prescription of anticancer drugs to cohorts of 28 tumor types reveals targeting opportunities. Cancer Cell *27*, 382–396.

Ryan, C.J., and Tindall, D.J. (2011). Androgen receptor rediscovered: the new biology and targeting the androgen receptor therapeutically. J. Clin. Oncol. *29*, 3651–3658.

Sboner, A., Demichelis, F., Calza, S., Pawitan, Y., Setlur, S.R., Hoshida, Y., Perner, S., Adami, H.O., Fall, K., Mucci, L.A., et al. (2010). Molecular sampling of prostate cancer: a dilemma for predicting disease progression. BMC Med. Genomics *3*, 8.

Scher, H.I., and Sawyers, C.L. (2005). Biology of progressive, castration-resistant prostate cancer: directed therapies targeting the androgen-receptor signaling axis. J. Clin. Oncol. *23*, 8253–8261.

Sharpless, N.E., and Depinho, R.A. (2006). The mighty mouse: genetically engineered mouse models in cancer drug development. Nat. Rev. Drug Discov. *5*, 741–754.

Shen, M.M., and Abate-Shen, C. (2010). Molecular genetics of prostate cancer: new prospects for old challenges. Genes Dev. *24*, 1967–2000.

Stanbrough, M., Bubley, G.J., Ross, K., Golub, T.R., Rubin, M.A., Penning, T.M., Febbo, P.G., and Balk, S.P. (2006). Increased expression of genes converting adrenal androgens to testosterone in androgen-independent prostate cancer. Cancer Res. *66*, 2815–2825.

Subramanian, A., Tamayo, P., Mootha, V.K., Mukherjee, S., Ebert, B.L., Gillette, M.A., Paulovich, A., Pomeroy, S.L., Golub, T.R., Lander, E.S., and Mesirov, J.P. (2005). Gene set enrichment analysis: a knowledge-based approach for interpreting genome-wide expression profiles. Proc. Natl. Acad. Sci. USA *102*, 15545–15550.

Taylor, B.S., Schultz, N., Hieronymus, H., Gopalan, A., Xiao, Y., Carver, B.S., Arora, V.K., Kaushik, P., Cerami, E., Reva, B., et al. (2010). Integrative genomic profiling of human prostate cancer. Cancer Cell *18*, 11–22.

Wang, Z.A., Mitrofanova, A., Bergren, S.K., Abate-Shen, C., Cardiff, R.D., Califano, A., and Shen, M.M. (2013). Lineage analysis of basal epithelial cells reveals their unexpected plasticity and supports a cell-of-origin model for prostate cancer heterogeneity. Nat. Cell Biol. *15*, 274–283.

Whitlock, M.C. (2005). Combining probability from independent tests: the weighted Z-method is superior to Fisher's approach. J. Evol. Biol. *18*, 1368–1373.

Wong, Y.N., Ferraldeschi, R., Attard, G., and de Bono, J. (2014). Evolution of androgen receptor targeted therapy for advanced prostate cancer. Nat. Rev. Clin. Oncol. *11*, 365–376.